

## Chapter 4

### DIII-D Contributions to the FY2013 Joint Research Target on ELM Control

M.E. Fenstermacher<sup>1</sup>, D.J. Battaglia<sup>2</sup>, K.H. Burrell<sup>3</sup>, J.M. Canik<sup>4</sup>, T.E. Evans<sup>3</sup>,  
A.M. Garofalo<sup>3</sup>, S.P. Gerhardt<sup>2</sup>, B.A. Grierson<sup>2</sup>, A.E. Hubbard<sup>5</sup>, R. Maingi<sup>2</sup>,  
D.M. Orlov<sup>6</sup>, T.H. Osborne<sup>3</sup>, M.W. Shafer<sup>4</sup>, W.M. Solomon<sup>2</sup>, and D.G. Whyte<sup>5</sup>

<sup>1</sup>Lawrence Livermore National Laboratory, Livermore, California

<sup>2</sup>Princeton Plasma Physics Laboratory, Princeton, New Jersey

<sup>3</sup>General Atomics, P.O. Box 85608, San Diego, California 92186-5608

<sup>4</sup>Massachusetts Institute of Technology, Cambridge, Massachusetts

<sup>5</sup>University of California San Diego, La Jolla, California

<b>1.0 Overview .....</b>	<b>46</b>
<b>2.0 Experiments and Analysis Focused on Particle Transport Physics Mechanisms</b>	<b>50</b>
<b>2.1 Effect of the EHO on Edge Particle Transport in QH-mode Plasmas .....</b>	<b>50</b>
2.1.1 Goals and Background.....	50
2.1.2 Results Contributing to JRT13 Goals .....	50
<b>2.2 Determining the RMP Fields Internal to the Plasma and Their Effect on Edge     Particle Transport .....</b>	<b>51</b>
2.2.1 Goals and Background.....	51
2.2.2 Results Contributing to JRT13 Goals .....	52
<b>2.3 Edge Particle Transport During I-mode Plasma Operation in DIII-D.....</b>	<b>53</b>
2.3.1 Goals and Background.....	53
2.3.2 Results Contributing to JRT13 Goals .....	54
<b>2.4 Conclusions .....</b>	<b>55</b>
<b>3.0 Experiments and Analysis Focused on Testing Physics Limits to Operating   Regimes .....</b>	<b>55</b>
<b>3.1 Exploring the I-mode Operating Space in DIII-D .....</b>	<b>55</b>
3.1.1 Goals and Background.....	55
3.1.2 Results Contributing to JRT13 Goals .....	56
<b>3.2 Extending QH-mode Operation to High Fusion Performance .....</b>	<b>59</b>
3.2.1 Goals and Background.....	59
3.2.2 Results Contributing to JRT13 Goals .....	60
<b>3.3 Exploring the Density and Collisionality Limits of QH-mode Operation .....</b>	<b>61</b>
3.3.1 Goals and Background.....	61
3.3.2 Results Contributing to JRT13 Goals .....	61
3.4.1 Goals and Background.....	62
3.4.2 Results Contributing to JRT13 Goals .....	63
<b>3.5 Extension of VH-mode High Performance Pedestals to Stationary Operation Using     RMP Fields.....</b>	<b>64</b>
3.5.1 Goals and Background.....	64
3.5.2 Results Contributing to JRT13 Goals .....	65
<b>3.6 Exploring Requirements for RMP ELM Suppression on DIII-D with Less Than 12 I-     coils.....</b>	<b>66</b>
3.6.1 Goals and Background.....	66

**3.7 Conclusions ..... 68**

**4.0 Paths for Future Exploration ..... 68**

**4.1 Experiments and Analysis Focused on Particle Transport Physics Mechanisms ..... 68**

    4.1.1 Future Experiments ..... 68

    4.1.2 Analysis ..... 68

**4.2 Experiments and Analysis Focused on Testing Physics Limits to Operating Regimes ..... 69**

    4.2.1 Future Experiments ..... 69

    4.2.2 Ongoing Analysis ..... 70

**Acknowledgment ..... 70**

**References ..... 70**

## 1.0 Overview

### 1.1 Summary of Report

The DIII-D requirements for the final quarterly milestone of the 2013 Joint Facilities Research Target (JRT13) have been met by the activities described below. The requirements of previous quarterly milestones have been met as documented in the following reports: 1) First quarterly milestone, report GA-C27505, 2) Second quarterly milestone, report GA-C27557, and third quarterly milestone, report GA-C27663. For the fourth quarterly milestone, the 2013 experiments required to address the goals of JRT13 have been executed and analysis has been performed. DIII-D contributions toward the development of high-performance stationary regimes devoid of large edge localized modes (ELMs) are summarized below in terms of both new understanding of the physical mechanisms that control edge pedestal transport, and achievement of extensions to the operating space of various stationary H-mode regimes without large uncontrolled Type-I ELMs.

The physics mechanisms that control edge pedestal transport, in particular particle transport, were explored with new diagnostic techniques in QH-mode, resonant magnetic perturbation (RMP) ELM controlled, and I-mode plasmas. Measurements of the impurity confinement time of fluorine injected into companion QH-mode and ELMing plasmas has demonstrated that the edge harmonic oscillation associated with QH-mode operation produces superior impurity flushing to ELMs, and moreover, the impurity confinement time does not increase as the toroidal rotation is reduced at constant density, despite significant improvements in the energy confinement. From very recent experiments, plasmas with strong  $n=1$  RMP fields and net-zero input torque showed clear indications of static resonant  $n=1$  islands in both MECH data and from Thomson  $T_e$  and electron cyclotron emission (ECE). Each of these latter diagnostics showed  $T_e$ -flattening near rational surfaces which could be related to particle transport increases through ExB convection effects. In a candidate I-mode plasma, for which a small increment in heating power leads to an edge transition, the edge temperature increases by a larger fraction than the increase in input power and simultaneously there is no change in the global or boundary density indicating that particle transport is not improved. Analysis of all of these recent observations is in progress.

The operating regimes of QH-mode, RMP ELM controlled and I-mode plasmas have been expanded by experiments done as part of this JRT. In QH-mode plasmas, simultaneous achievement of high beta, high confinement and low  $q_{95}$  needed for ITER  $Q=10$  performance was demonstrated for 18 energy confinement times, with modest levels of neutral beam torque. Also the operating space of QH-mode plasmas was expanded to higher fractions of the Greenwald density (up to 80% in highly shaped configurations) as needed for high density operation in ITER. RMP ELM suppression

was obtained in new experiment with a range of I-coil sets (12, 11, and 10 I-coils) and extrapolation of these results shows that the ITER ELM coil system may be able to tolerate a loss of up to five of its 27 coils, while leaving a sufficient margin of current in the remaining coils to still meet the DIII-D ELM suppression criterion. Additional experiments with 9, 8, 7, and 5 I-coils were also done during the writing of this report. Finally, a large space was explored, including scans of plasma current, safety factor  $q_{95}$ , lower triangularity, and elongation, to study the response of observed I-mode regimes to these global plasma parameters, to map the H-mode threshold in this atypical magnetic topology with ion  $\nabla B$  drift out of the divertor, and to determine the “operating window” of the regime.

## 1.2 Introduction

Operation of future tokamak devices with H-mode confinement and the associated strong edge pedestal pressure gradients, including ITER and power reactors, must include systems to control ELM instabilities in order to achieve acceptably low levels of plasma facing component (PFC) erosion. In ITER the erosion of divertor target PFCs caused by uncontrolled Type-I ELMs is predicted to limit the lifetime of these components to several hundred full power discharges. The erosion due to ELMs in a power reactor will be more than an order of magnitude greater than in ITER. Techniques to reliably reduce or eliminate PFC erosion from ELMs are critical to the viability of these future devices.

The 2013 Joint Facilities Research Target (JRT) focuses the combined resources of the NSTX, C-Mod and DIII-D programs on understanding the physics mechanisms for and extending the operating space of multiple techniques of stationary tokamak operation without large uncontrolled Type-I ELMs. The text of the 2013 JRT and the associated quarterly milestones are below

### Annual Target

Conduct experiments and analysis on major fusion facilities to evaluate stationary enhanced confinement regimes without large ELMs and to improve understanding of the underlying physical mechanisms that allow acceptable edge particle transport while maintaining a strong thermal transport barrier. Mechanisms to be investigated can include intrinsic continuous edge plasma modes and externally applied 3D fields. Candidate regimes and techniques have been pioneered by each of the three major US facilities (C-Mod, D3D and NSTX). Coordinated experiments, measurements, and analysis will be carried out to assess and understand the operational space for the regimes. Exploiting the complementary parameters and tools of the devices, joint teams will aim to more closely approach key dimensionless parameters of ITER, and to identify correlations between edge fluctuations and transport. The role of rotation will be investigated. The research will strengthen the basis for extrapolation of stationary regimes which combine high

energy confinement with good particle and impurity control, to ITER and other future fusion facilities for which avoidance of large ELMs is a critical issue.

### Quarter Milestones

**1st Quarter Milestone.** Begin analysis of previously collected data with a goal of defining new experiments. Develop an initial plan for collaborative experiments and analysis in the 2nd half of the fiscal year.

**2nd Quarter Milestone.** Utilize data analysis to define a final plan for experiments in the 2nd half of FY-13 on at least a single facility, including diagnostic and operations requirements.

**3rd Quarter Milestone.** Begin planned experiments on at least a single facility. Evaluate results, including comparisons to previous data, and adjust analysis and experimental plans as necessary.

**4th Quarter Milestone.** Complete the required experiments and analysis. Prepare a joint report summarizing the contributions toward the development of high-performance stationary regimes devoid of large ELMs, and identifying important paths for future exploration.

There is a duality to the objectives of JRT2013: it includes both investigation of the underlying physics mechanisms that control edge pedestal transport (in particular particle transport) during ELM control techniques, and exploration of the possible extension of the operating regimes of various techniques to a broader range of tokamak operating parameters, which also tests the governing physics mechanisms.

The DIII-D program has contributed to the completion of JRT 2013 through both the execution and analysis of multiple experiments focused on several of the leading ELM control techniques. Multiple experiments have been executed using QH-mode plasmas, I-mode operating regimes, VH-mode plasmas, and resonant magnetic perturbation (RMP) ELM control techniques. Experiments have been focused on both aspects of JRT2013 vis: some have targeted the detailed mechanisms controlling edge particle transport during ELM control and others have concentrated on expanding the operating regimes for various techniques. A summary of the experiments executed within the scope of JRT2103 is given in Table IV.1.2-1

Table IV.1.2-1 DIII-D Experiments in 2013 Contributing to JRT13 Goals. Research Areas: B&PP: Boundary and Pedestal Physics, D&C: Dynamics and Control; JRT13 Goals: TPM: Transport Physics Mechanisms, PE: Performance Extension

Regime	Title	Research Area	JRT13 Goal
I-mode/ T-III ELMs	Density transport in small and no ELM regimes: Compare Type III ELMy H-mode, I-phase, and “I-mode candidate” in DIII-D	B&PP	PE
I-mode/ T-III ELMs	Density transport in small and no ELM regimes: Compare Type III ELMy H-mode, I-phase, and “I-mode candidate” in DIII-D	B&PP	TPM
RMP	Measure dependence of magnetic island ExB convective transport as a function of toroidal rotation	B&PP	TPM — Not completed
RMP	Study $n = 3$ RMP transport asymmetries with applied RMP phase FLIPS to identify and document conditions that minimize pedestal pressure reduction	B&PP	TPM
RMP	RMP ELM suppression with less than 12 I-coils for ITER	B&PP	PE
VH-mode/ RMP	Extend VH-mode duration using 3D fields from the I-coil and C-coil and document the pedestal properties	B&PP	PE
QH-mode	Determine edge harmonic oscillation (EHO)-induced particle transport rates at ITER-relevant conditions	D&C	TPM
QH-mode	QH-mode creation and sustainment with ITER-relevant $co-I_p$ NBI torque	D&C	PE
QH-mode	Sustain low torque QH-mode at high normalized Fusion performance for alternate to ITER baseline	D&C	PE
QH-mode	Density and collisionality dependence of EHO	D&C	TPM & PE

The organization of this report is aligned with the requirements of JRT2013, vis. Section 2 describes experiments and analysis focused on effects of various techniques on edge transport, Section 3 concentrates on experiments and analysis that test the physics limits of operating regimes for various techniques, and Section 4 summarizes paths for future exploration indicated by the work done this year.

## 2.0 Experiments and Analysis Focused on Particle Transport Physics Mechanisms

### 2.1 Effect of the EHO on Edge Particle Transport in QH-mode Plasmas

#### 2.1.1 Goals and Background

The primary goal of this experiment was to determine the rate at which a non-intrinsic, non-recycling impurity is transported out of a QH-mode plasma for a range of experimental conditions, and to contrast this rate with that in ELMing H-modes. QH-mode conditions are theoretically predicted to be maintained by the edge harmonic oscillation (EHO), and this experiment focused on quantifying the particle transport rates in the presence of an EHO, including the possible effect of neoclassical ion transport in the edge of QH-mode plasmas (see the JRT appendix). This is an important issue for ITER in which all ELM control techniques must show that core accumulation of tungsten sputtered in the divertor region can be prevented.

The key experimental technique used in the experiment to directly measure the edge impurity particle confinement was the injection of multiple short pulses of carbon tetrafluoride ( $\text{CF}_4$ ) gas and the monitoring of the decay of the fluorine in the edge pedestal with the charge exchange recombination (CER) system tuned to a fluorine line. The experimental conditions were optimized to include a set of EHO mode numbers from  $n=1, 2, 3$  and broadband fluctuations. Further, the dependence on plasma density, toroidal rotation and applied 3D magnetic perturbations were used to assess the particle transport. Shot-by-shot scans of parameters were done, with other global variables fixed when possible. ELMing versions of these QH-mode conditions were also produced throughout the experiment, and data from these periods are being analyzed for comparison with the high priority QH-mode measurements. In all cases more comprehensive measurements were acquired for detailed modeling of the particle transport [ $E_r$  and motional Stark effect (MSE) for equilibrium, BES, UF-CHERS for turbulent fluctuations], besides the gross observable of the particle confinement time  $\tau_p$  from the simple decay of the fluorine charge-exchange emission intensity.

#### 2.1.2 Results Contributing to JRT13 Goals

Measurements of the impurity confinement time of non-intrinsic, non-recycling fluorine injected into companion QH-mode and ELMing plasmas has demonstrated that the edge harmonic oscillation associated with QH-mode operation produces superior impurity flushing to ELMs, and moreover, the impurity confinement time does not increase as the toroidal rotation is reduced at constant density, despite significant improvements in the energy confinement. Fluorine particle confinement time as a function of plasma line-averaged density (Fig. IV.2.1-1) shows that in the QH-mode phases the impurity particle confinement is lower than in the ELMing phase, suggesting better impurity flushing from the plasma by the EHO than by ELMs. Fluorine particle

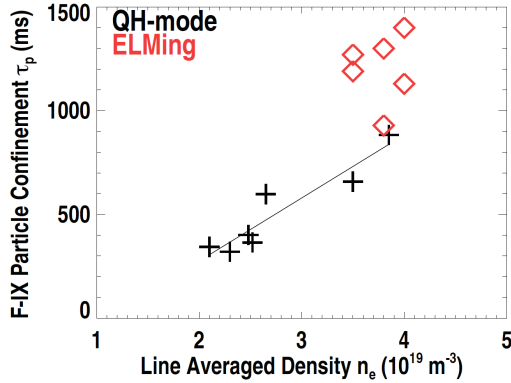


Fig. IV.2.1-1. Fluorine particle confinement time vs line-averaged density for ELMing H-mode and QH-mode operation.

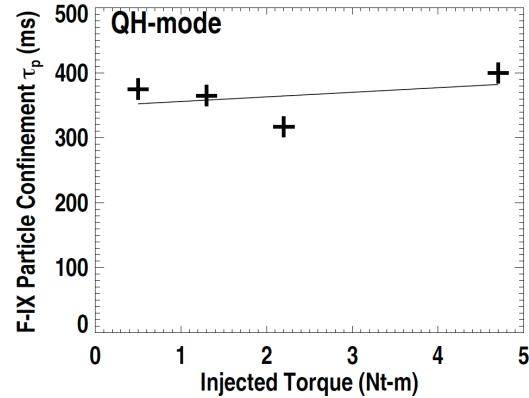


Fig. IV.2.1-2. Fluorine particle confinement time vs injected neutral beam torque for QH-mode operation at constant density.

confinement as a function of injected NB

torque during QH-mode operation at fixed density (Fig. IV.2.1-2) shows little dependence on the input torque. Edge ( $\Psi_N=0.8$ ) toroidal rotation varies a factor of 5 (10–50 km/s) and central rotation varies more than a factor of 50 (2–120 km/s) from the low to high end of this torque scan. These results are particularly important because there is concern that ELM-suppressed regimes may lead to impurity accumulation without the flushing typically associated with ELMing conditions. This experiment shows that the impurity flushing in QH-mode is higher than in ELMing H-mode.

## 2.2 Determining the RMP Fields Internal to the Plasma and Their Effect on Edge Particle Transport

### 2.2.1 Goals and Background

The purpose of this experiment was to examine the plasma response to 3D non-axisymmetric magnetic perturbations as part of efforts to build a comprehensive model of the self-consistent fields internal to the plasma and the effect of those fields on edge particle transport, under application of external resonant magnetic perturbation (RMP) fields. The experiment examined the changes in topology, transport (particle and energy) and turbulence using  $n=1$  magnetic perturbations in inner-wall limited (IWL) plasmas. Although not optimized for RMP ELM suppression, the applied fields were predicted to generate the largest magnetic island structures possible within DIII-D plasmas. In combination with IWL plasmas, these  $n=1$  perturbations allowed for better diagnostic access to test plasma response models, similar to previous work in O. Schmitz *et al.*, Nucl. Fusion **52**, 043005 (2012). This experiment took advantage of advancements in diagnostic access, numerical modeling and experimental tools. The plan was to advance validation of vacuum and resistive MHD calculations of self-consistent internal fields by comparing data against synthetic diagnostic results from the code simulations, and to

eventually fold that predictive capability for the internal fields into code simulations of the effect on particle transport based on several different theoretical mechanisms.

Application of RMPs is a robust ELM control technique on DIII-D [1]. However, the understanding of this process is incomplete, and it is crucial to develop predictive capability of this technique for ITER. A current working theory is that the RMP creates some mechanism that restricts the inward pedestal growth, preventing the pedestal from reaching a peeling-ballooning limit [2]. One proposed mechanism is that an island is formed at the top of the pedestal due to the RMP fields, and this is supported by recent resistive two-fluid linear MHD modeling [3]. This modeling suggests that screening of the externally applied RMP fields by the plasma is diminished where perpendicular electron flow is low, which is possible at the top of the pedestal. This is in contrast to vacuum modeling, which suggests high levels of stochasticity throughout the pedestal.

To enhance the ability to measure the contrast between the vacuum model predictions and the full plasma response prediction of the RMP fields in the plasma, the experiment was designed with IWL plasma shape and strong  $n=1$  RMP fields applied by the C-coil. Lower  $n$  (as opposed to  $n=3$ ) reduces the “pileup” of neighboring resonant surfaces. Similarly, limited plasmas reduce edge shear to reduce the pileup as well. This simplifies the modeling of the plasma response for a particular surface. This also allows better diagnostic access of outboard midplane measurements. Another key benefit is the reduction of the strong separatrix deformation from homoclinic tangles (which requires an X-point). A key technique featured in this experiment was the use of modulated electron cyclotron heating (MECH) power. ECH pulses have been used successfully in LHD and TEXTOR to study changes in the magnetic topology, i.e., nested flux surfaces, small isolated magnetic islands, mixed islands and stochastic layers and regions of strong stochasticity, due to intrinsic resonant magnetic fields and applied RMP fields [4–6]. The experiment also used differential phase-locked imaging with the tangential filtered X-point soft x-ray (SXR) camera, similar to previous successful techniques in  $n=3$  RMP ELM suppression experiments. Images using a low energy filter ( $T_e \geq \sim 40$  eV) show lobe structures consistent with vacuum calculations. Conversely, using a higher energy filter ( $T_e \geq \sim 400$  eV), images show helical kink-like displacements localized in the steep gradient region consistent with calculations with the linear resistive two-fluid MHD code, M3D-C1 [3]. Similar to the differential phase-locked imaging, traveling  $n=1$  waves were also used for better access by midplane visible cameras and ECEI.

### 2.2.2 Results Contributing to JRT13 Goals

This experiment was completed less than a week before the deadline for submission of this report, but based on control-room analysis, seemingly clear indications of static resonant  $n=1$  islands were observed in Thomson  $T_e$  and electron cyclotron emission (ECE) at net-zero input torque. Each of these diagnostics show  $T_e$ -flattening near rational surfaces. By increasing the torque slightly, the island signatures went away – potentially

giving a first indication of resonant screening of non-axisymmetric fields via rotation. Proper evaluation of relevant rotation quantities will be needed to determine the details of the apparent screening effects. Scientists from NIFS (Ida and Ohdachi) who collaborated on this experiment used modulation ECH to probe the same plasmas and corroborated the location of islands O- and X-points. The change in radial propagation speed of MECH pulses helped to indicate the difference between nested flux surfaces, islands and stochastic regions. Also, IWL H-modes were found at low power, which was unexpected. This was highly dependent on C-coil phase. Further analysis showed that the favorable C-coil phase in H-mode was consistent with the standard error field correction phase. Reciprocating probe measurements in the backend low-power phase showed degradation of floating potential gradient (possible increasing stochasticity) and plasma potential (possible increase of ion loss) as perturbation current is increased. Further analysis will be done as follow-up to the 2013 JRT.

### 2.3 Edge Particle Transport During I-mode Plasma Operation in DIII-D

#### 2.3.1 Goals and Background

The goal of this experiment was to explore and characterize the particle and thermal transport features of ELM-free regimes for comparison to the other facilities. A magnetic configuration with the ion grad-B drift pointed away from the primary X-point was used, i.e. a topology with “unfavorable” power access to H-mode, but which has been used to explore I-mode in C-Mod. The experimental plan used steps of neutral beam input power within a shot to explore the parameter space of I-mode/small-ELM regimes and the transition to H-mode (Fig. IV.2.3-1). A large suite of boundary fluctuation diagnostics was simultaneously focused on these plasmas in order to obtain more complete information on the role of small-scale MHD in regulating particle and energy transport. The fluctuation diagnostics data will be critical in determining any bifurcations in pedestal/core fluctuation behavior that are expected to occur at an L-I-mode transition (based on observations from ASDEX-Upgrade and C-Mod).

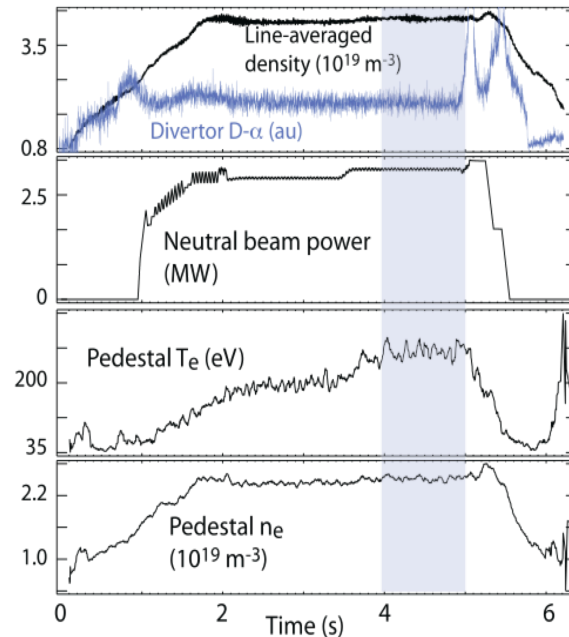


Fig. IV.2.3-1. Example shot (#153023) where a candidate I-mode appears (the shaded region). A substantial (>25%) increase in pedestal  $T_e$  occurs with constant core and pedestal density with a <10% increase in injected power. The recycling  $D_\alpha$  light in the divertor indicates that no H-mode transition or ELM activity occurs.

### 2.3.2 Results Contributing to JRT13 Goals

A candidate I-mode phase is shown in Fig. IV.2.3-1 where a small increment in heating power leads to an edge transition, i.e. where the edge temperature increases by a larger fraction than the increase in input power. Simultaneously there is no change in the global or boundary density. It is just such a transition in energy transport, and the formation of a  $T_e$  pedestal, in the absence of improved particle confinement, which is the key feature of I-mode. The development of a boundary temperature/energy barrier is evident in Fig. IV.2.3-2 in the candidate I-mode phase. While no standard H-mode transition occurs, the  $D_\alpha$  recycling light indicates complex behavior that evolves throughout the different phases, as do related density fluctuations in the pedestal from the BES diagnostic. These fluctuations are presently being analyzed and being compared to Type-III ELM regimes.

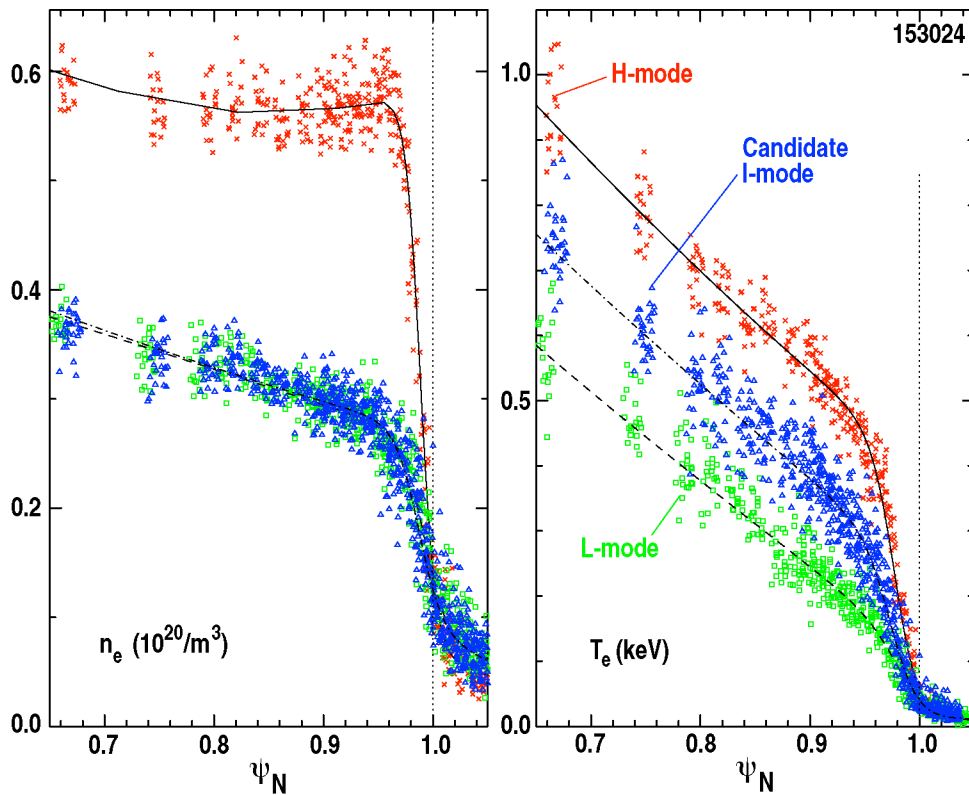


Fig IV.2.3-2. Example edge profile (#153050) comparing boundary  $T_e$  profiles between a standard L-mode with no pedestal and a candidate I-mode phase where an edge thermal barrier begins forming with only a small increment in beam heating.

## 2.4 Conclusions

The experiments and analysis focused on the physics controlling the edge particle transport pioneered new diagnostic techniques to make direct measurements of impurity particle confinement and the effects of externally applied fields on internal magnetic and plasma profiles. Measurements of fluorine transport from short puffs of  $\text{CF}_4$  was and will be an important technique to directly measure impurity confinement in stationary regimes without large ELMs. MECH is a valuable technique to explore the internal magnetic structure within these plasmas. The data and analysis to date certainly suggest that the role of 3D magnetic fields could be a common feature of the particle transport control in QH-mode, RMP ELM control and I-mode plasmas. At this point further analysis is still required to determine the details of commonality in the physics mechanisms that control the edge particle transport in these regimes.

## 3.0 Experiments and Analysis Focused on Testing Physics Limits to Operating Regimes

### 3.1 Exploring the I-mode Operating Space in DIII-D

#### 3.1.1 Goals and Background

The goal of this experiment was to explore the operating space near the parameters of a previous DIII-D discharge from last year that showed I-mode characteristics. The strategy was to alter parameters that are known to affect (or avoid) transition into a standard H-mode, namely density, X-point position, and plasma current. This scan occupied the first half-day.

The second part of the experimental plan was focused on using the best discharge of the first run and providing further exploration of the regime. Options included: 1) varying the input beam in order to examine the role of input torque, 2) exchanging the NBI heating with ECH to both examine the role of torque and direct electron heating, 3) varying the magnetic balance to examine the role of the H-mode power threshold and/or threshold for obtaining Type-III ELMs, 4) Exploring the accessibility/maintainability space of I-mode with respect to density, in particular the ability to raise the density once in I-mode through simple gas fuelling while simultaneously increasing the power including the boundary fluctuation response to density/power scans, and 5) closer examination of pedestal particle transport by local particle balance (edge filterscopes), which required an outer gap scan, and/or modification to puffing location. We also considered non-perturbing argon puffing to assess particle transport.

DIII-D experiments carried out in 2012 with ion grad-B drift pointed away from the primary X-point, showed that a temperature barrier was forming in the absence of a density barrier, a key feature of the I-mode regime. The most promising discharge (#149908) was part of a large scoping study exploring access to I-mode and thus small

variations near the conditions of 149908 were not explored in detail. Analysis of edge density fluctuations indicated that small-scale instabilities were present including 2–4 kHz bursts in recycling, as well as higher frequency ~50 kHz precursor events. It was speculated that such edge modes were responsible for strong particle transport and inhibited the formation of density pedestal. These fluctuation features have some qualitative resemblance to those in low density Type-III ELMy H-modes. Discovering commonalities to small ELM and no-ELM regimes is a central theme to the 2013 JRT. This experiment was designed to expand our limited set of fluctuation data for this candidate I-mode regime in DIII-D and compare with measurements from Type-III ELMing H-mode.

### 3.1.2 Results Contributing to JRT13 Goals

A large space was explored in the DIII-D experiment to study the response of this no/small ELM regime to global plasma parameters, to map the H-mode threshold in this atypical magnetic topology, and to determine the “operating window” of the regime. A graphical summary of the parameter scan in plasma density versus input beam power is shown in Fig. IV.3.1-1.

The parameter scans also included: 1) plasma current:

1–1.5 MA, 2) safety factor  $q_{95}$ :

3.3–5.2, 3) lower triangularity:

0.37–0.72, and 4) elongation:

1.62–1.72. It is noted from

Fig. IV.3.1-2 that the

“unfavorable” topology leads to

a substantial increase in the allowed input power before H-mode is accessed, which would typically occur on DIII-D at ~1.5 MW for the  $B_T=2$  T used in the experiment. It is apparent that both shaping and density play roles in determining the H-mode threshold, a result qualitatively consistent with previous experience.

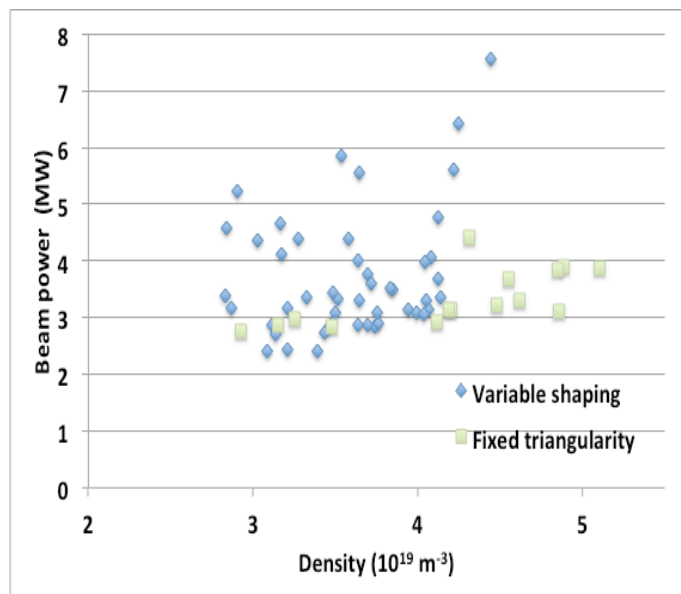


Fig. IV.3.1-1. Parameter space of core density vs input beam power covered in the experiment. All points are either in L-mode or candidate I-mode phases. No H-modes are shown. All plasmas have a lower single null shape. The “fixed triangularity” cases have a lower triangularity of 0.53.

While candidate I-mode slices were identified, the overall DIII-D energy confinement improvement was modest, with a maximum  $H_{98y2} \sim 0.75$ . Preliminary assessment shows that the expected evolution of the  $T_e$  pedestal is cut short by H-mode transitions, which are occurring at a relatively earlier stage in the pedestal formation than seen in C-Mod or ASDEX-Upgrade. The cause of the  $T_e$  pedestal termination appears to be sawteeth heat pulses. The importance of sawteeth is shown in Fig. IV.3.1-2 where the highest pedestal  $T_e$  is found at the lowest plasma current.

The sawteeth heat pulses are substantially smaller at lower current (higher safety factor), which allows the candidate I-mode phase to reach higher  $T_e$  before the H-mode. This effect is strong enough on DIII-D to counter the expected degradation in confinement/pedestal height at the lower plasma current, which is seen on C-Mod. This result suggests that sawtooth suppression/control may be more important than high plasma current to accessing higher performance I-mode phases in DIII-D.

From the discharge this year the scaling of the power threshold for the I- to H-mode transition shows similarities with previous scalings found for the threshold from Type-III to Type-I ELMs. Figure IV.3.1-3 shows the I-H threshold power (and that threshold power normalized to the ITER L-H power threshold scaling) as functions of density normalized to the square of the poloidal field. These data were taken for discharges at a fixed shape and toroidal field by scanning the plasma current. The shape of the I-H threshold power is similar to the previous scaling of TIII – TI ELMing regime transition power scaling of  $P_{\text{TIII-TI}} \sim I_p^{2.4} / n_e^2$  [7].

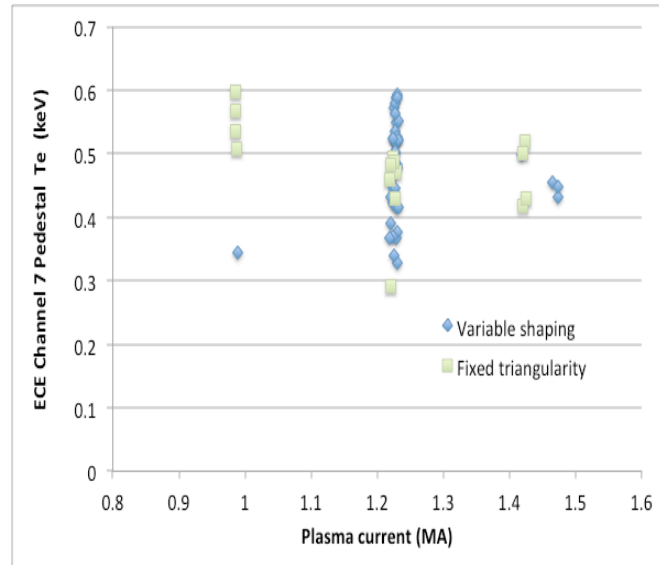


Fig. IV.3.1-2. Achieved edge/pedestal  $T_e$  (measured with ECE channel 7) vs plasma current. All plasmas lower single null before any H-mode transition. The green squares have a constant lower triangularity of 0.53.

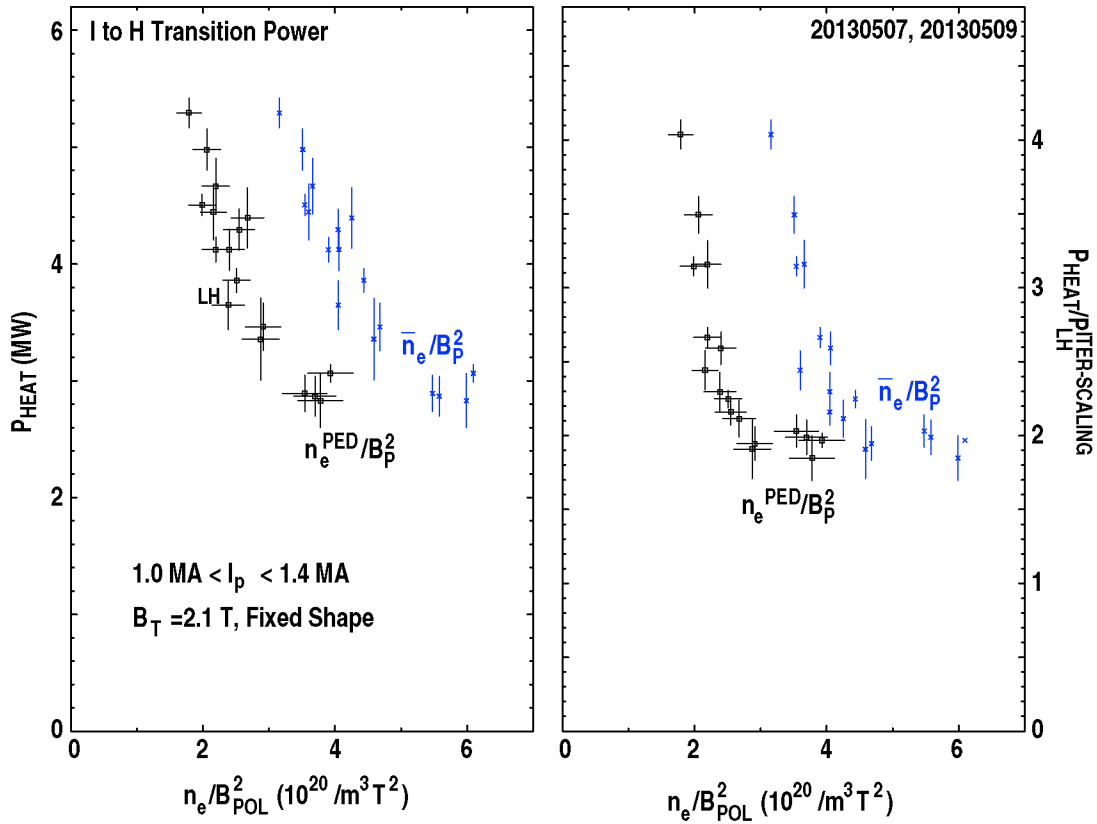


Fig. IV.3.1-3. I-H transition power threshold (MW and normalized to ITER L-H power threshold scaling) as functions of density normalized to (poloidal field)<sup>2</sup>.

Comparison of pedestal characteristics important to stability analysis between I-mode and ELMing H-mode cases show the I-mode is significantly away from stability boundaries that produce ELMs. Figure IV.3.1-4 shows normalized pedestal electron temperature, normalized pedestal total pressure, and pedestal alpha parameter (pressure gradient) all as functions of density normalized to poloidal field. The I-mode cases are at lower temperature, lower pressure and lower pressure gradient than comparable H-mode cases. Figure IV.3.1-4 also shows that the I-mode pedestals are significantly wider than comparable ELMing H-mode pedestals, and wider than suggested by EPED scaling.

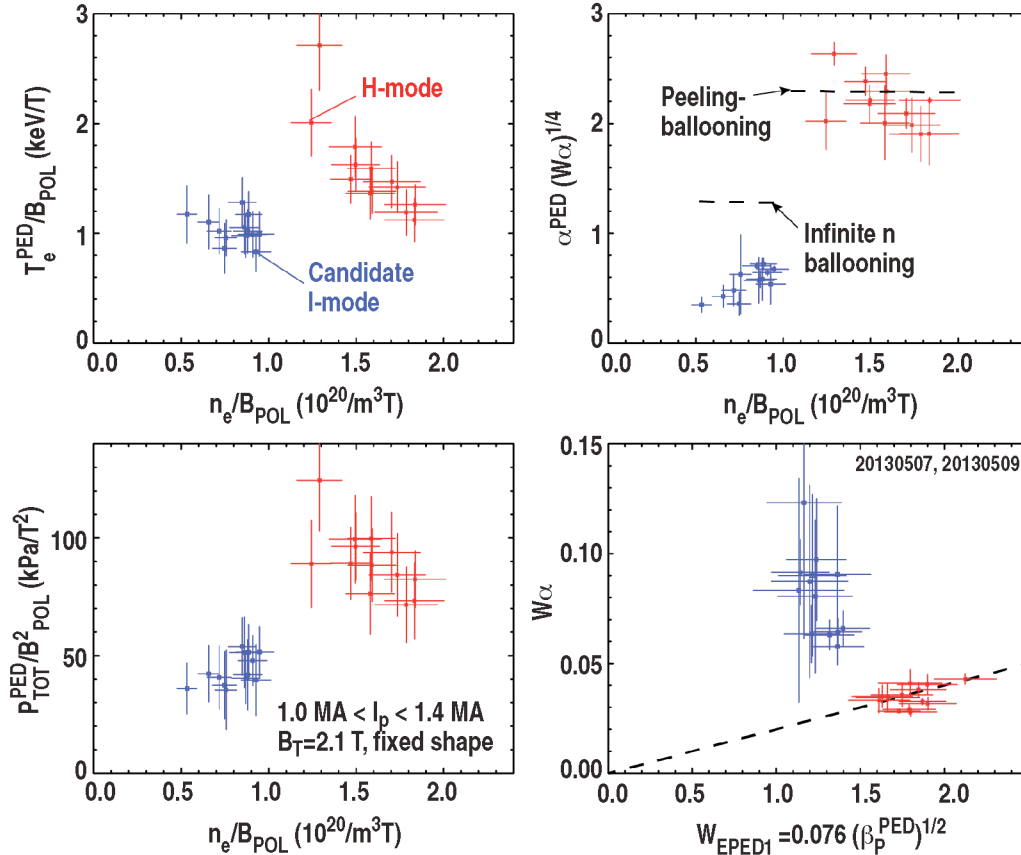


Fig. IV.3.1-4. Pedestal parameters important to stability analysis for DIII-D I-mode vs comparable ELMing H-mode cases.

## 3.2 Extending QH-mode Operation to High Fusion Performance

### 3.2.1 Goals and Background

The experiment to sustain low torque QH-mode at high normalized fusion performance, as an alternate to ITER baseline, focused on extending the operational space of the QH-mode regime to overlap with key constraints associated with ITER baseline operation, in particular the low values of  $q_{95}$  and co- $I_p$  input torque simultaneous with good confinement ( $H_{89p}=2$ ) and moderate normalized beta ( $\beta_N \sim 2$ ). The goal was to obtain a value of the normalized fusion performance parameter  $G = \beta_N H_{89p} / q_{95}^2 \sim 0.4$  sustained in QH-mode for duration  $> 5\tau_L$  with net NBI torque between 0 and 1 Nm.

QH-mode experiments in November 2012 achieved for the first time QH-mode operation at high fusion performance parameter  $G=0.4$  with very low NBI torque. These experiments were carried out with forward  $I_p$  and reversed  $B_T$ , and used an upper biased DND plasma cross section, C-coil  $n=3$  operation at 7 kA to produce the edge rotation shear required for QH-mode, RWM feedback operation using I-coils, and a recent boronization of the DIII-D vessel. The value of  $G=0.4$  was achieved only briefly, before a locked mode terminated the high beta phase. Furthermore, the value of  $G=0.4$  was

achieved with NBI torque in the counter direction, although at very low level of about 0.5 Nm.

The new experiment, focused on the JRT goals, aimed more simply at reaching low  $q_{95}$  at the moderate  $\beta_N \sim 1.8\text{--}2.0$  of the ITER baseline scenario. Without a specific reason for off-axis current drive from the tilted NB line, the proposed experiment operated in the more established counter-rotating QH-mode with reversed  $I_p$  and forward  $B_T$ .

### 3.2.2 Results Contributing to JRT13 Goals

Simultaneous achievement of high beta, high confinement and low  $q_{95}$  needed for ITER  $Q=10$  performance was demonstrated for 18 energy confinement times, with modest levels of neutral beam torque. QH-mode at normalized fusion performance corresponding to  $Q=10$  in the ITER baseline scenario (i.e.  $\beta_N H_{89p} / q_{95}^2 \sim 0.4$ ) was easily obtained at  $q_{95} \sim 3.2$ , but only with counter neutral beam injection (NBI) torque. High performance QH-mode operation was obtained in both USN and LSN plasmas shapes as shown in Figs. IV.3.2-1 and IV.3.2-2. Reducing the counter- $I_p$  torque led to a locked mode in these initial experiments. The torque threshold for locked modes is lower at higher  $q_{95}$ , and at  $q_{95} \sim 4.7$  the NBI torque can be reduced to zero without locked modes. Improved error field correction using resistive wall mode (RWM) feedback should be a promising tool to overcome the locked mode limitation. Increasing the density was not attempted in the time available, but this would have a strong impact on the locked mode behavior.

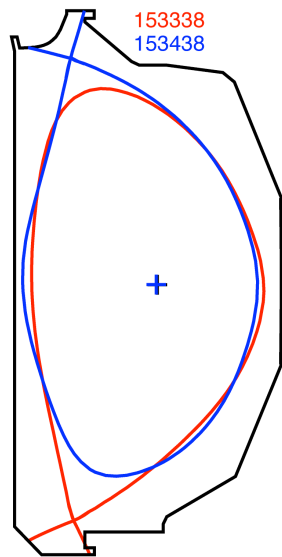


Fig. IV.3.2-1. USN (blue) vs LSN (red) shapes used for high performance QH-mode experiments.

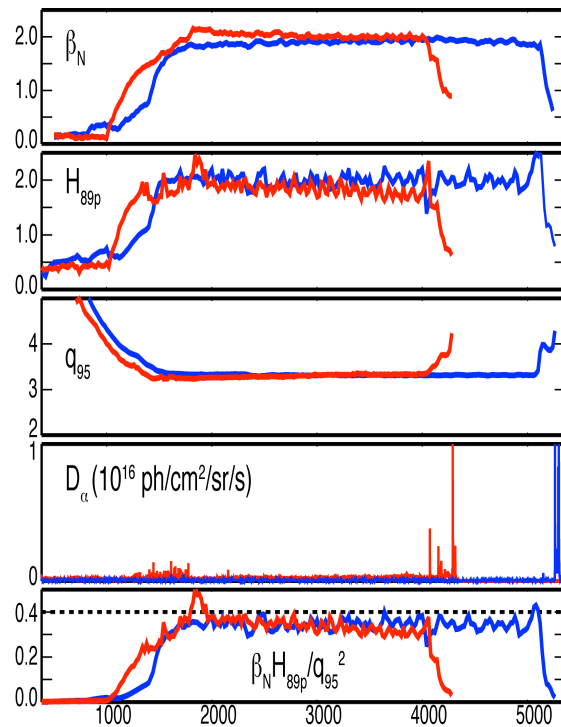


Fig. IV.3.2-2. Comparison of high fusion performance QH-mode plasmas in both USN (blue) and LSN (red) shape.

### 3.3 Exploring the Density and Collisionality Limits of QH-mode Operation

#### 3.3.1 Goals and Background

There were two major goals for this experiment, viz.: 1) to investigate the physics of the QH-mode density limit, in particular to show that access to QH-mode is not correlated with Greenwald fraction, consistent with model predictions, and that collisionality (via its effect on bootstrap current) is the relevant density parameter, and 2) to document the EHO mode structure under the wide range of conditions and compare with both linear eigenmode calculations as well as calculations from the nonlinear MHD code JOEK. The experiment was also designed to test model predictions for how the plasma shape and rotation influence the density limit. In particular the experiment was designed to acquire data related to the rotation requirements for the EHO, which will be used in simulations to help demonstrate that the EHO is indeed a peeling mode saturated by edge rotational shear. These were important JRT13 related steps to improve the confidence that QH-mode can be accessed in ITER at high Greenwald fraction, as predicted.

Experiments have previously shown that increased shaping can increase the QH-mode density limit, and reduced rotation appears to reduce the particle transport driven by the EHO, also leading to higher density QH-modes. However, the highest density QH-modes on DIII-D are still at relatively low Greenwald fractions ( $n/n_G \sim 0.6$ ) compared with ITER requirements. Hence, an often-cited concern is that QH-mode may not be ITER relevant. Stability to ELMs is thought to be maintained via increased particle transport driven by the EHO. There have been various efforts to investigate the EHO mode structure, but no systematic effort has been made to compare with predicted mode structures, so relevant data was collected in this experiment, particularly as part of a  $q_{95}$  scan which changed the mode structure. Previously, the shear in the rotation driven by the radial electric field,  $\omega_E = E_r/RB_\theta$  was found to be an important parameter for QH-mode operation [8]. This work argued that the appropriate non-dimensional quantity involved normalizing to the Alfvén frequency. This experiment explored different toroidal fields as part of the density/collisionality variations to test this rotation normalization also.

#### 3.3.2 Results Contributing to JRT13 Goals

Consistent with the JRT13 goal to explore and expand the boundaries of operating spaces for stationary regimes without ELMs toward more ITER relevant conditions, these experiments expanded the operating space associated with QH-mode plasmas to higher fractions of the Greenwald density as needed for high density operation in ITER. The density requirements for QH-mode access were investigated and no correlation with Greenwald fraction was found. Indeed, with high shaping, Greenwald fractions exceeding 80% have now been achieved (Figs IV.3.3-1 and IV.3.3-2), and density can be controlled during the QH-mode phase with either pellets or gas puffing. High density QH-mode

operation is qualitatively consistent with modeling using the ELITE code, indicating that strong shaping expands the kink/peeling stability boundary to higher pressure and current, allowing access to higher densities without destabilizing ELMs. Importantly, calculations with both the EPED and ELITE codes predict that the expected density on ITER is compatible with QH-mode operation in the ITER shape.

### 3.4 Developing QH-mode Creation and Sustainment Scenarios with Low Co- $I_p$ Torque

#### 3.4.1 Goals and Background

The goal of this experiment was to investigate techniques to create and sustain QH-mode with NBI torque levels relevant to next-step devices such as ITER. Work in the 2011 and 2012 campaigns demonstrated sustained QH-mode operation with ITER relevant NBI torque in the range of 0 to 1 Nm; however, the QH-mode was initiated in these shots using large, counter- $I_p$  torques in the range of -3 to -5 Nm. The focus of the present experiment was creation of the QH-mode at low NBI torque.

Experiments over the past three years have demonstrated that the NTV torque from non-axisymmetric magnetic fields with toroidal mode number  $n=3$  can be used to sustain QH-mode plasmas even when the NBI torque is in the range of 0 to 1.3 Nm (in the co- $I_p$  direction) [9–11]. Several different I- and C-coil configurations were used in this work. Taking the best features of the various configurations, the optimum non-axisymmetric coil configuration uses the C-coil

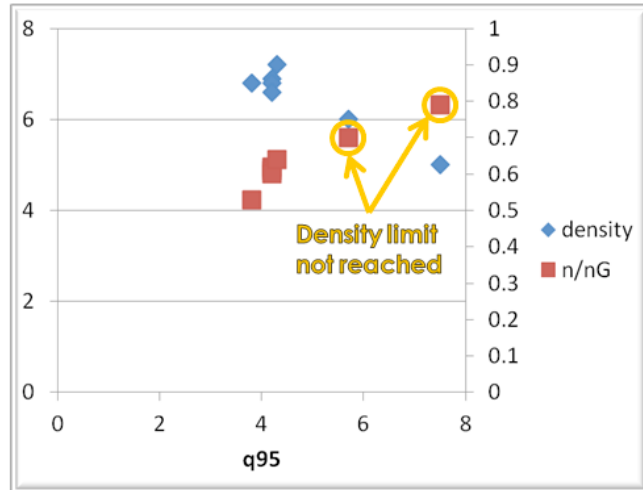


Fig. IV.3.3-1. Density and Greenwald density fraction achieved during QH-mode operation as functions of  $q_{95}$ . For the discharges above  $q_{95}=5$  the actual limit was not reached and is likely higher than shown.

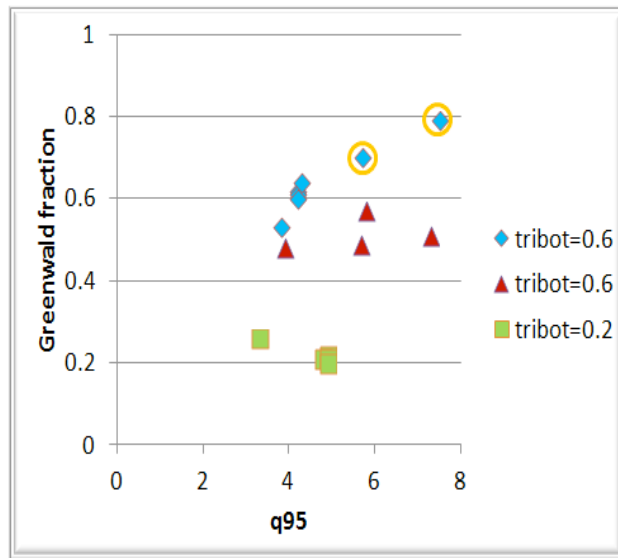


Fig. IV.3.3-2. Greenwald density fraction achieved during QH-mode operation as functions of  $q_{95}$  for three plasma triangularity values. Higher shaping allows higher density limit.

to generate  $n=3$  fields and the I-coil for  $n=1$  error field correction and some odd parity  $n=3$  contribution.

Some experiments on low torque startup for QH-mode were carried out in the 2012 campaign. Several lessons were learned from these shots. First, simply replacing the counter- $I_p$  beam program with an equivalent power waveform made up of balanced beams did not work; significant problems were seen with locked modes. The usual QH-mode NBI starts at 300 ms during the current ramp up phase of the discharge. We were able to establish an Ohmic current ramp phase, which satisfies the need to have no NBI torque during this part of the shot. This lesson forms the basis for the present experiment, which used Ohmic current ramp up. Second, even starting with balanced beams in current flattop, the plasma rotates in the co- $I_p$  direction, possibly due to the intrinsic torque. Even with the slightly counter- $I_p$  NBI torque (-0.2 Nm) later in shots like 149083, locked modes occurred as the initially co- $I_p$  rotation slowed towards zero. Shots in the 149083 series were run with neoclassical tearing viscosity (NTV) torque initiated well after the L to H transition. Accordingly, the lesson is that we should turn on the coils providing the NTV torque prior to the L to H transition if possible. Third, there was insufficient time in the 2012 run after developing the Ohmic startup to find the lower density limit. Since QH-mode operates better at lower densities, we need to see how low the Ohmic target density can go. The challenge in the present experiment was to find techniques that allowed us to move the plasma from one stationary operating mode with zero NBI torque to another. The Ohmic plasma operates with no NBI torque and exhibits a core rotation which is typically counter- $I_p$  (around -10 km/s) and a pedestal rotation which is co- $I_p$  (around +10 km/s). The QH-mode with added NTV torque can operate with zero net NBI torque and with rotation which is basically counter everywhere (typically -30 km/s) except perhaps at the magnetic axis and at the separatrix. As the beam power turns on, two processes occur which push the plasma rotation in opposite directions. The intrinsic rotation is equivalent to a co- $I_p$  torque while the NTV torque from the  $n=3$  fields is a counter- $I_p$  torque. Our previous experiments show that in the final, QH-mode stationary state at  $\beta_N = 1.8$ , the NTV torque is significantly larger. The issue for the present experiment was to find a way for the NTV torque to exceed the intrinsic torque during the dynamic phase after the L to H transition.

#### 3.4.2 Results Contributing to JRT13 Goals

Several aspects of a low-torque startup scenario for QH-mode access in ITER were developed, but a complete scenario will require higher edge ion temperatures than achieved in the experiment this year. A first successful aspect of the scenario shown by this experiment was that there was no obvious effect of the non-resonant  $n=3$  fields on the L to H transition. However, based on work with NTV torque over the past three years, a small torque initially when  $\beta_N$  was low was expected to change to a counter- $I_p$  torque as  $\beta_N$  rose. Instead the torque due to the  $n=3$  fields was about 1 Nm in the co- $I_p$

direction at 300 ms after the beams came on. The explanation may be that the pedestal temperatures in these plasmas were quite low compared to the ones run previously ( $<1$  keV initially versus 3–5 keV). The neoclassical offset velocity might be so close to zero that the NTV torque was co- $I_p$  for the rotation speeds of this experiment. If this was the case, a scenario will need to be created with higher pedestal ion temperature while still maintaining low torque conditions. This experiment was also successful in providing clear lessons to guide future experiments, including showing that: 1) loss of the IU90 portion of I-coil leads to more severe mode locking problems when the I-coil is used to do  $n=1$  error field correction plus producing some  $n=3$  field with 60 degree phasing, 2) possibly because of the low edge ion temperature, magnetic torque on the plasma from the  $n=3$  fields was in the co- $I_p$  direction during this experiment rather than the desired counter- $I_p$  torque, and thus Ohmic operation into the  $I_p$  flat top accordingly resulted in no ITER compatible source of counter- $I_p$  torque, 3) future low torque experiments will need to return to early NBI during the  $I_p$  ramp to obtain higher pedestal  $T_i$ , including possible investigate of the use of feedback controlled ECH during the current ramp to control the q-profile evolution and avoid locked modes.

### **3.5 Extension of VH-mode High Performance Pedestals to Stationary Operation Using RMP Fields**

#### *3.5.1 Goals and Background*

The primary goal of this experiment was to reproduce as closely as possible the best VH-mode performance observed in DIII-D and then to apply 3D perturbation fields in order to control the density rise and to extend the duration of the mode or to avoid the termination event entirely. Previous attempts in 2005 focused on applying  $n=3$  I-coil fields during the onset of the VH-mode in the ELM-free H-mode phase. Those experiments found that relatively small I-coil currents resulted in good density control during the early VH-mode phases but triggered fast growing  $n=1$  and  $n=2$  modes that terminated the discharges. The purpose of this experiment was to extend the duration of VH-modes using 3D magnetic perturbation fields in double null plasmas.

Confinement regimes that are devoid of ELMs and have core parameters exceeding those in ELMing H-modes are referred to as VH- and EP H-modes in DIII-D [12–15] and NSTX [16, 17] respectively. These modes have enhanced levels of stored energy, expanded pedestal widths, higher edge bootstrap currents, larger total noninductive current fractions, broader poloidal flow shear regions, reduced thermal diffusivities just inside the top of the pedestal and suppressed density fluctuations near the top of the pedestal compared to typical H-mode plasmas. Unfortunately, these modes are transient and therefore have no practical utility for fusion reactor applications unless techniques can be developed to avoid the uncontrolled increase in the plasma  $\beta$  and subsequent MHD events leading to the termination phase. While VH-modes and EP H-modes have significant similarities, there are differences in the dynamics leading up to the triggering

and termination of these regimes as discussed in Ref. [17]. In VH-modes the energy confinement can reach values that exceed typical L-mode and H-mode confinement by a factor of 3.5 and 1.8 respectively with low radiative fractions and core impurity concentrations. Peak axial triple products ( $n_D T_i \tau_E$ ) of  $4 \text{ \AA} \times 10^{23} \text{ m}^{-3} \cdot \text{eV} \cdot \text{s}$  [14] have been obtained in these plasmas.

In DIII-D the best VH-modes are obtained with low recycling wall conditions such as those following a boronization and a high-temperature bake of the vessel walls. In one of the best VH-mode discharges obtained in DIII-D,  $\beta_N$  reached  $\sim 3.2$  shortly after  $P_{inj}$  is increased from  $\sim 2.5$  MW to  $\sim 8$  MW. The line average density continued to increase while  $\beta_N$  saturated and started to degrade. The lower divertor  $D_a$  recycling emission showed several strong bursts during the rising density phase followed by a series of ELM-like events that appeared to be involved in the termination of the VH-mode. This dropped the discharge into an ELM-free phase with several sporadic ELMs followed by a final ELM-free or reduced  $\beta_N$  VH-mode.

In NSTX, the onset dynamics and evolution of the EP H-mode differ significantly from those in DIII-D VH-modes. Here, the beam power is ramped up to  $\sim 5.2$  MW while the plasma current is being ramped up and then dropped to  $\sim 4$  MW during the  $I_p$  plateau from  $t = 200$  ms to the end of the discharge. Initially, the discharge is relatively ELM-free and the line average density as well as the global stored energy ( $W_{MHD}$ ) and the thermal energy confinement time ( $\tau_E$ ) rise continuously until  $\sim 430$  ms in the discharge when they roll over and trigger a large ELM-like event. Subsequently the EP H-mode is triggered following a second large ELM-like event at  $\sim 550$  ms, which initially causes a loss in the stored energy and density to a lesser extent. During the EP H-mode there is a significant increase in the stored energy and confinement time while the density increases slowly relative to the other confinement parameters. The termination phase seems to result from a slow reduction of  $\tau_E$  that ends with a strong  $D_a$  burst.

### 3.5.2 Results Contributing to JRT13 Goals

The goals of this experiment to produce high-quality VH-modes and improve their diagnosis, were successful, with several good examples of VH-modes produced (based on their high confinement and  $\beta_N$ ; a second transition to VH-mode wasn't obvious, and detailed profile analysis needs to be done to confirm), and fluctuation measurements taken with FIR, BES, and DBS. Several attempts were made to control the VH-mode with  $n=3$  fields, with the perturbation initiated during the L-mode phase, during the ELM-free phase before VH, and during the VH-mode itself. None of these showed an extended duration of the VH-mode, however, and instead it appeared that the 3D fields hastened the onset of ELMs a bit during VH-mode. Further, density pump-out was not observed during the ELM-free phase, possibly due to the relatively high collisionality and  $q_{95}$  of these plasmas.

Data from this experiment is being used to: 1) Evaluate the effects of 3D fields on the pedestal plasma profiles and stability during VH-modes including effects on kinetic profiles ( $T_e$  and  $T_i$ ),  $\omega_E$ , rotation profiles and edge fluctuations, 2) Compare the characteristics of VH-modes and termination events in DIII-D with those of enhanced pedestal (EP) H-modes in NSTX, and 3) Provide data for 3D two-fluid, extended MHD and full-f kinetic transport codes as well as for 3D stellerator-symmetric equilibrium codes. The measurements are being supplemented by an analysis of the stability properties of the edge plasma. This is partially motivated by the recent progress in understanding ELM suppression via RMP application, and if successful will guide later experiments on NSTX-U and DIII-D aiming to control and extend the duration of the EP H-mode and VH-mode.

### **3.6 Exploring Requirements for RMP ELM Suppression on DIII-D with Less Than 12 I-coils**

#### *3.6.1 Goals and Background*

The purpose of this experiment was to obtain Type-I ELM suppression in low density low collisionality ITER-similar shape H-mode plasmas with reduced (<12) set of I-coils. The key questions to be addressed included: 1) Obtain ELM suppression with reduced number of I-coils and determine the I-coil current amplitude needed for ELM suppression, 2) Determine the minimum number of I-coils needed for ELM suppression to provide guidance to ITER for ELM control coil malfunctions, 3) Determine the effect of error field correction on ELM suppression with reduced number of I-coils, and, 4) Demonstrate recovery of ELM suppression after coil malfunctions. These are very critical questions for ITER ELM Control Coils design.

Our previous simulations [18] showed that an application of  $n=3$  or  $n=4$  toroidal perturbation in the ITER ELM coils will be able to produce a stochastic layer in the pedestal region of similar or greater width than in DIII-D. Vacuum island overlap width (VIOW) parameter [19] in these simulations exceeded 16.5% of radial width in normalized poloidal flux coordinates. According to our previous findings [20], this width of the pedestal stochastic region is typically correlated with the suppression of large Type I ELM in DIII-D. It was also adapted by ITER as a design criterion for ITER ELM coils

Recently, we have performed extensive numerical simulations to assess the performance of the ITER ELM coils in case of individual coil malfunctions. The vacuum simulation predict that ITER ELM coils as currently designed will be able to exceed the DIII-D ELM suppression criterion even with malfunctions of eight midplane ELM coils if coil currents are adjusted in the other coils [19]. This experiment was designed to test these model predictions by applying RMP ELM suppression fields to the same DIII-D plasma using 12, 11, 10, 9 etc. of the available I-coils on DIII-D.

### 3.6.2 Results Contributing to JRT13 Goals

The new results from this experiment suggest that the coil currents required for ELM suppression were no greater with the reduced coil sets than is typically required for the full set. An example of ELM suppression with 11 I-coils (black) and with 10 I-coils (red) is shown in Fig. IV.3.6-1. In these discharges ELMs are suppressed in the case with 10 I-coils earlier in the phase with coil current of 3 kA than in the case with 11 I-coils. This counter-intuitive result could provide an important validation of recent modeling [18,19] of the physical mechanisms involved. This modeling shows that the spectral sidebands introduced by deactivating individual coils can often increase the magnetic stochasticity within the plasma, thereby increasing transport and facilitating ELM suppression. Deactivating individual coils results not only in the reduction of the dominant  $n=3$  component of the perturbation field, but also in a significant increase in the amplitudes of  $n=1$  and  $n=2$  sidebands. These sidebands may also be amplified by the plasma response. Application to ITER finds that the ITER ELM coils may be able to tolerate a loss of up to five of its 27 coils, while leaving a sufficient margin of current in the remaining coils to still meet the DIII-D ELM suppression criterion. Further, the new experiments show that the presence of the spectral sidebands does not adversely affect the plasma rotation or confinement. As these experiments and additional ones using 9, 8, 7, and 5 I-coils were completed only a few days before the end of the JRT13 period, analysis with both vacuum and two-fluid modeling is still underway to interpret and understand these data. Results will be presented in an APS post-deadline invited talk and in several planned publications.

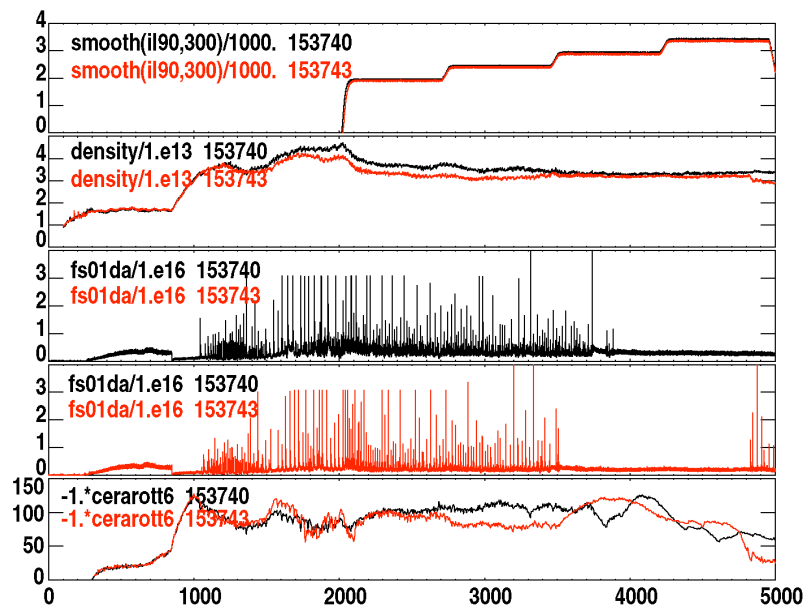


Fig. IV.3.6-1. Time history of I-coil current, density (line average and pedestal), inner divertor  $D_{\alpha}$  emission and pedestal rotation for RMP ELM suppression discharges with 11 and 10 I-coils.

### 3.7 Conclusions

The experiments and analysis focused on testing the physics limits to operating regimes for several stationary H-mode regimes without ELMs succeeded in finding control parameters that allowed expansion of the operating spaces. For QH-mode a high degree of shaping allowed higher density operation and sustained high fusion performance was obtained with a moderate input torque. For RMP ELM suppression optimization of the I-coil current allowed suppression with reduced number of I-coils. In I-mode operation lower plasma current allowed operation to higher pedestal temperature due to reduced sawteeth amplitude. The common feature of these results may be the effect of the actuator on preventing the expansion of the pedestal pressure (either width or height) to the ELM instability boundary. But clearly differences remain in the detailed physics that accomplishes this pedestal control: in QH-mode it is done by an internally generated mode the EHO, in the RMP case the control comes by way of externally applied 3D fields, and for the I-mode it appears to be necessary to control the power flow through the pedestal to stay in I-mode and avoid the H-mode transition.

## 4.0 Paths for Future Exploration

### 4.1 Experiments and Analysis Focused on Particle Transport Physics Mechanisms

#### 4.1.1 Future Experiments

Progress has been made during the JRT13 work toward understanding the physics mechanisms controlling edge particle transport in stationary regimes without ELMs, but complete understanding of the fundamental issue of how ELMs are prevented in these regimes (e.g. by the EHO, or the external application of 3D fields, or by other internal plasma modes) will likely require additional experiments. Results from the JRT13 work indicate that two new techniques used in the DIII-D experiment this year, viz.: 1) short puffs of CF<sub>4</sub> with CER tuned to fluorine lines and, 2) the monitoring of the plasma response to modulated ECH beams, show promise for providing data to validate models of the physics mechanisms driving edge particle transport in stationary H-mode regimes without Type-I ELMs. These two techniques, combined with comprehensive fluctuations and turbulence diagnostics, could be applied in future experiments at all three facilities to investigate the edge particle transport mechanisms in I-mode, QH-mode, RMP ELM control, EP H-mode and other ELM control regimes.

#### 4.1.2 Analysis

Given that many of the experiments addressing the JRT13 goal of increasing understanding of the physics mechanisms driving edge particle transport were executed less than a few months before the end of the JRT13 period, considerable analysis is still ongoing. Significant modeling of the impurity transport in the QH-mode experiments with the CF<sub>4</sub> puffs needs to be done. The data from injection of modulated ECH into a

plasma with strong RMP fields is being analyzed with techniques pioneered by our colleagues at LHD in Japan. Finally investigations into the connections between variations in edge turbulence and fluctuations measurements, and changes in the edge transport (e.g. through the pedestal density) are underway especially for the I-mode operation, but also for all the stationary regimes without ELMs, and will continue well after the JRT13 period.

## 4.2 Experiments and Analysis Focused on Testing Physics Limits to Operating Regimes

### 4.2.1 Future Experiments

Results from the DIII-D experiments during JRT13 that were focused on extending the operating regimes of various stationary regimes without ELMs showed that future experiments need to target specific aspects of the regimes. These are summarized below organized by operating mode.

To further extend the QH-mode operational space to low torque startup, a scenario must be developed that maintains high edge pedestal ion temperature during the early plasma current ramp-up phase so that the NTV torque will be strongly counter- $I_p$  and provide sufficient edge rotation shear to access QH-mode with low torque input. Ideas to achieve this include application of NB heating very early in the discharge and possible use of ECH under feedback control during the current ramp to affect the current profile evolution and avoid early locked modes. To further extend QH-mode to high fusion performance at low input torque ( $\beta_N * H_{89}/q_{95}^2 = 0.4$  at 0 – 1 Nm input torque), techniques for improved error field correction must be developed to overcome the tendency of these scenarios toward locked modes as  $q_{95}$  is reduced for maximization of the fusion performance metric  $G = \beta_N * H_{89}/q_{95}^2$ . Resistive wall mode (RWM) feedback techniques are a good candidate for this improved error field correction. Also higher density may help to increase  $G$  by allowing low  $q_{95}$  operation without locked modes, providing the confinement factor  $H_{89}$  does not decrease as much as the gains in going to low  $q_{95}$ . The experiments this year did show that it should be possible to obtain QH-mode at ITER relevant densities and Greenwald fractions, but further experiments which attempt to maintain QH-mode operation at these very high density conditions for many energy confinement times are still needed.

To extend the I-mode operating space in DIII-D requires that sawteeth energy pulsed through the edge pedestal be reduced or eliminated. I-mode operation is close enough to ELMing H-mode in DIII-D that sawteeth heat pulses passing through candidate I-mode temperature pedestals frequently trigger a transition into the H-mode. There was evidence for a correlation between smaller sawteeth heat pulses in candidate discharges at lower plasma current and higher  $T_e$  pedestals in I-mode-like conditions having no evidence of a density pedestal. Various techniques are effective for reducing the size of sawteeth including central ion cyclotron resonance frequency (ICRF) power and off-axis

current drive or counter NB injection to keep the central safety factor above 1.0. In DIII-D the actuators for off-axis current drive include off-axis neutral beam current drive (NBCD) using the tilted beamlines, and electron cyclotron current drive (ECCD) tuned to off-axis deposition.

Future experiments to extend the performance of RMP ELM suppression to fewer I-coils will need to concentrate on understanding the effects of  $n=1$  and  $n=2$  sidebands in the applied mode spectrum when additional I-coils are turned off. The working hypothesis of ELM suppression with some I-coils missing is that  $n=1$  and  $n=2$  sidebands help to fill in gaps in the spectrum of perturbation fields in the plasma and thereby prevent the growth of the width of the pedestal to the ELM instability boundary. Clearly this mechanism must breakdown as the number of coils continues to be reduced and the resonant  $n=3$  components of the spectrum become smaller. The clear path to optimization of the combined  $n=1$ ,  $n=2$  and  $n=3$  spectrum will not be able to be developed until the physics mechanisms controlling the edge particle transport and the growth of the pedestal width during RMP application are understood.

#### 4.2.2 Ongoing Analysis

The primary tool of ongoing analysis for the experiments extending the operating regimes is pedestal stability calculations with the ELITE and EPED code packages. For the DIII-D I-mode candidates, the density/Greenwald fraction limit QH-modes and the RMP ELM suppression cases with less than 12 I-coils, the analysis will start with kinetic EFITS which are used by ELITE to determine how close the pedestal operating point is to the ballooning, peeling-ballooning or kink-peeling stability boundaries. Analysis with EPED will then determine how close the pedestal pressure width and height are from the intersection of the peeling-ballooning and kinetic ballooning stability boundaries. Similar analysis is ongoing for C-Mod I-mode cases and plasmas in EP H-mode in NSTX, to compare with the DIII-D results. These tests of the proximity of the pedestal operating points to various instability boundaries will give information on the direction to push the pedestal in order to increase its performance without triggering ELMs.

### Acknowledgment

This work was supported by the US Department of Energy under DE-AC52-07NA27344, DE-AC02-09CH11466, DE-FG02-04ER54698, DE-AC05-00OR22725, DE-FG02-04ER54762, and DE-FG02-05EAR54809.

### References

- [1] T.E. Evans *et al.*, Nature of Physics **2**, 419 (2006).
- [2] P.B. Snyder *et al.*, Phys. Plasmas **19**, 056115 (2012).
- [3] N.M. Ferraro, Phys. Plasmas **19**, 056105 (2012).
- [4] K. Ida, *et al.*, Phys. Rev. Lett. **100** 045003 (2008).

- [5] K. Ida *et al.*, *New J. Phys.* **15** 013061 (2013).
- [6] O. Schmitz, Personal Communication (2012).
- [7] T.H. Osborne, et al., *Scaling of ELM and H-mode pedestal characteristics in ITER shape discharges in the DIII-D tokamak*, Proceedings of the 24th EPS Conference on Controlled Fusion and Plasma Physics, June 9–13, 1997, Berchtesgaden, Germany, General Atomics report GA-A22638, July 1997.
- [8] A.M. Garofalo, *Nucl. Fusion* **51**, 083018 (2011).
- [9] K.H. Burrell *et al.*, *Phys. Plasmas* **19**, 056117 (2012).
- [10] A.M. Garofalo *et al.*, "High Beta, High Confinement, Stationary ELM-free Operation at Low Plasma Rotation," Proceedings of 39th European Physical Society Conference On Plasma Physics, Stockholm, Sweden, (2012), <http://ocs.ciemat.es/epsicpp2012pap/pdf/O2.102.pdf>.
- [11] K.H. Burrell *et al.*, "Quiescent H-mode Operation Using Torque from Non-axisymmetric, Non-resonant Magnetic Fields," *Nucl. Fusion* **53** (to be published)
- [12] G.L. Jackson *et al.*, *Phys. Rev. Lett.* **67**, 30981 (1991).
- [13] S.I. Lippmann, *et al.*, *J. Nucl. Mater.* **196-198**, 498 (1992).
- [14] T.H. Osborne *et al.*, *Nucl. Fusion* **35**, 23 (1995).
- [15] T.E. Evans, *et al.*, *J. Nucl. Mater.* **220-222**, 235 (1995).
- [16] R. Maingi *et al.*, *J. Nucl. Mater.* **390-391**, 440 (2009).
- [17] R. Maingi *et al.*, *Phys. Rev. Lett.* **105**, 135004 (2010).
- [18] D.M. Orlov, *et al.*, *Fusion Eng. Design* **87**, 1536 (2012).
- [19] T.E. Evans, *et al.*, *Nucl. Fusion* **53**, 093029 (2013).
- [20] M.E. Fenstermacher, *et al.*, *Phys. Plasmas* **15**, 056122 (2008)